IEEE Access
Multidisciplinary | Rapid Review | Open Access Journal

Received June 26, 2019, accepted July 6, 2019, date of publication July 9, 2019, date of current version July 26, 2019.

*Digital Object Identifier 10.1109/ACCESS.2019.2927658*

# Absorptive/Transmissive Frequency Selective Surface With Wide Absorption Band

**QINGXIN GUO[1], (Senior Member, IEEE), JIANXUN SU[1], ZENGRUI LI[1], (Member, IEEE), LAMAR Y. YANG[2], (Senior Member, IEEE), AND JIMING SONG[3], (Fellow, IEEE)**

[1]School of Information Engineering, Communication University of China, Beijing 100024, China
[2]Department of Electrical and Computer Engineering, University of Nebraska-Lincoln, Lincoln, NE 68588, USA
[3]Department of Electrical and Computer Engineering, Iowa State University, Ames, IA 50011, USA

Corresponding authors: Qingxin Guo (qxguo@cuc.edu.cn) and Jianxun Su (sujianxun_jlgx@163.com)

This work was supported in part by the National Natural Science Foundation of China under Grant 61671415 and Grant 61331002, and in part by the Fundamental Research Funds for the Central Universities of China.

**ABSTRACT** An absorptive/transmissive frequency selective surface (ATFSS) with absorption bands at both sides of a passband is presented. Equivalent circuits of the ATFSS that consists of a lossy frequency selective surface (FSS) and a lossless FSS were modeled. To improve the rejection at an undesired band, a transmission zero was introduced and controlled by loading the lossless FSS with four-legged loaded slots. The parasitic passband was suppressed when the cross structure in the lossless FSS was loaded with resistance. In order to expand the absorption band, loaded dipoles were utilized for the lossy FSS design. An ATFSS with wide absorption bands was realized after three ATFSSs with different performances were investigated. The proposed ATFSS was fabricated and measured. The measurement results showed that a passband at around 5 GHz with a minimum insertion loss of 0.92 dB was obtained. Within an ultrawide band from 2.8 to 11.4 GHz with $|S_{11}| < -10$ dB, the absorption rates of higher than 80% were obtained at a lower absorption band, from 2.7 to 3.8 GHz, and at a higher absorption band, from 6.2 to 11.7 GHz. Our results showed good agreements between the measurements and simulations.

**INDEX TERMS** Absorptive/transmissive frequency selective surface, ultra-wideband absorber, frequency selective rasorber, radar absorber.

## I. INTRODUCTION

Absorptive/transmissive frequency selective surface (ATFSS), which exhibits the characteristics of being transparent to incident electromagnetic waves in certain passbands and absorptive outside of the passbands, has attracted growing attentions during recent years. It is often referred to as a frequency selective rasorber (FSR) [1], which is a combination of the words radome and absorber, because it can be regarded as a radar absorber with transparent windows. A conceptual design of an absorptive/transmissive radome was proposed in [2]. Later on, a complete conceptual rasorber design of multilayer structures was presented in [1]. Recently, the concept of a 3-D FSR was presented in [3]. The ATFSS can be used to reduce the radar cross-sections (RCS) of stealthy radomes over a wide frequency band or to decrease the mutual interference among different subsystems that make up large communication systems. Ideally, a low RCS radome can transmit the in-band wave and absorb the incoming out-of-band wave, which is a unique characteristic of the ATFSS.

In general, an ATFSS with a two-layer structure consists of one layer of absorptive FSS, which acts as an absorber, and another layer of bandpass FSS, which functions as a filter. The absorber transmits in-band wave, absorbs part of the incident wave of the out-of-band signals, and mitigates the waves reflected by the second layer. The filter is transparent to the incident wave in a certain band while reflecting at the other frequencies for which it acts as a ground plane. Universal designs of an ATFSS which use two or three layers of a frequency selective surface (FSS) with certain spacing between them have been reported in some literatures. The absorption band can be higher than the transmission window [4]–[6], or lower than the transmission window [7], [8], or on both sides of a passband [9]–[13]. The absorptive FSS can be realized with different periodic structures, such as dipole [14], tripole [15], four-legged loaded [16], hexoganal ring [17], circular ring [18], and their

The associate editor coordinating the review of this manuscript and approving it for publication was Nosherwan Shoaib.

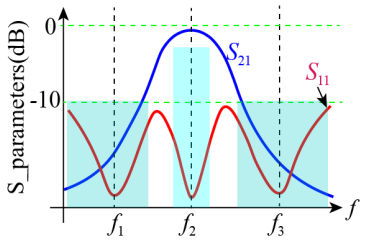


**FIGURE 1.** Response of an ATFSS.

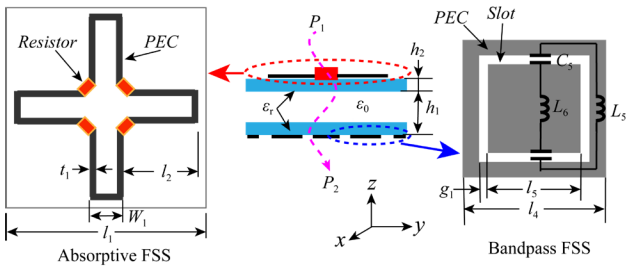


**FIGURE 2.** Configuration of ATFSS#1.

deformed structures [19]. The filter for most of the presented two-layer ATFSS was designed with slot elements.

This paper presents an ATFSS with a transparent window between two absorption bands based on the design of cascading of an absorber and a filter. Four-legged loaded elements and square slots were used in the design of the absorber and the filter. We proposed an equivalent circuit for the four-legged element with lumped resistors to accurately depict the performance of the absorptive FSS. To improve the out-of-band rejection at a desired band, a resistive cross was added into the filter FSS. Loaded dipoles were used to supplement the absorptive FSS for expanding the upper absorption band. After meticulously design, a passband at around 5 GHz was obtained between a lower absorption band from 2.7 to 3.8 GHz and a higher absorption band from 6.2 to 11.7 GHz.

## II. STRUCTURE AND SIMULATION RESULTS

As shown in Fig. 1, a typical response of an ATFSS is that $|S_{11}| = 0$ and $|S_{21}| = 1$ at $f_2$, while $|S_{11}| = 0$ and $|S_{21}| = 0$ at $f_1$ and $f_3$ [15], where $S_{11}$ and $S_{21}$ are the reflection coefficient and transmission coefficient of the ATFSS. The results imply that there is a transmission band with low insertion loss locates at around $f_2$, and two absorption bands around $f_1$ and $f_3$ at which the coefficients of both reflection and transmission coefficients are small.

### A. ORIGINAL ATFSS

Based on the design idea in [1] and referred to the work presented in [16], we initially designed an ATFSS (ATFSS#1) whose configuration is shown in Fig. 2. The left shows the structure of the absorptive FSS. It consists of one four-legged loaded cross element (or cross-frame element [16]) and four lumped resistors. Each corner near the center of the four legs

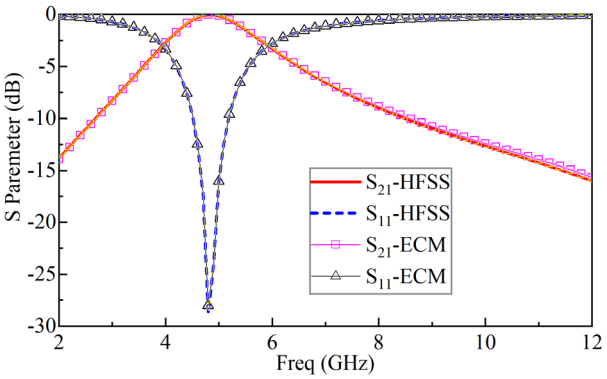


**FIGURE 3.** S parameters of the bandpass FSS.

is broken and connected with one lumped resistor for an absorptive feature. The loop needs to parallel resonate at $f_2$. The total length of each leg $(2l_2 + W_1)$ was initially set as $\lambda_0/(2\lambda_0/(2\sqrt{\varepsilon_{\text{eff}}}))$ at $f_2$, where $\varepsilon_{\text{eff}}$ is the effective permittivity of the substrate.

The absorptive FSS and the bandpass FSS are cascaded with an air gap to construct a two-layered ATFSS. Each FSS is supported with a substrate of $h_2 = 0.8$ mm thickness, permittivity of 4.5, and loss tangent of 0.0035. The space between them is denoted by $h_1$. The electrical length between two FSSs is approximately equal to $h_1 + 2h_2\sqrt{\varepsilon_{\text{eff}}}$, which is initially set as $\lambda_0/4$ at $f_2$ but less than $\lambda_0/4$ after considering the performances of the ATFSS. The dimensions of the structure are $l_1 = 25$ mm, $l_2 = 10$ mm, $l_4 = 12.5$ mm, $l_5 = 10$ mm, $W_1 = 2.5$ mm, $t_1 = 0.5$ mm, $g_1 = 0.3$ mm, $h_1 = 8.4$ mm, $h_2 = 0.8$ mm, respectively.

The bandpass FSS is shown on the right in Fig. 2. Square ring slots were chosen. The cell size of the filter FSS was only one quarter of that of the absorber, with $l_4 = l_1/2$. Both the inner side length of the slot ($l_5$) and the width of the slot ($g_1$) affected the center frequency of the filter, while $g_1$ determined the bandwidth of the passband. The square loop slot was modelled by a parallel-series circuit consisting of $L_5$, $C_5$ and $L_6$ ($L_5$ played a main role due to $L_5 >> L_6$), where $L_5 = 2.565$ nH, $L_6 = 0.035$ nH, $C_5 = 0.391$ pF. Fig. 3 shows the simulated S parameters of the filter by using the ECM and HFSS.

The equivalent circuit model (ECM) of the cross-frame loop without lumped resistors has been constructed by a series-parallel resonance circuit which consists of a series circuit ($L_1$ and $C_1$) and a parallel circuit ($L_2$ and $C_2$) [20], as shown in the left of Fig. 4(a). After the lumped resistors were inserted into the structure, designers might take it for granted that the ECM can be modelled by a revised circuit which is shown in the right of Fig. 4(a) [16]. Both ECMs are accurate at the low frequencies, but they cannot accurately depict the performance of the FSS at high frequencies, namely, the simulation results of the ECM are very different from the results obtained using the full-wave simulations, especially at high frequencies. One possible reason might be that the whole loop

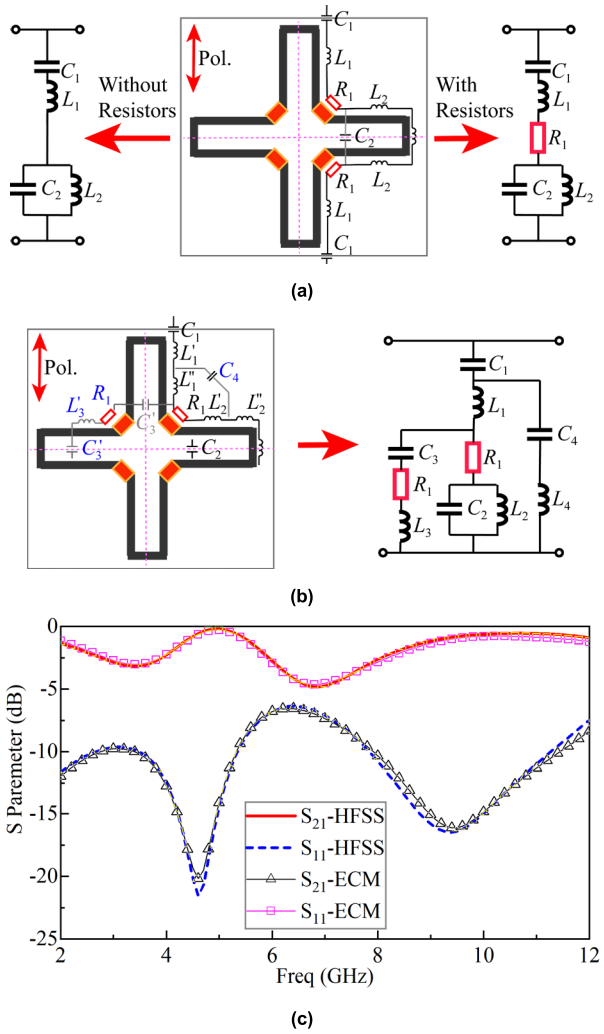


**FIGURE 4.** Equivalent circuits models and simulation results of the four-legged loaded cross element. (a) Original ECM. (b) Modified ECM. (c) Comparing results between the modified ECM and HFSS.

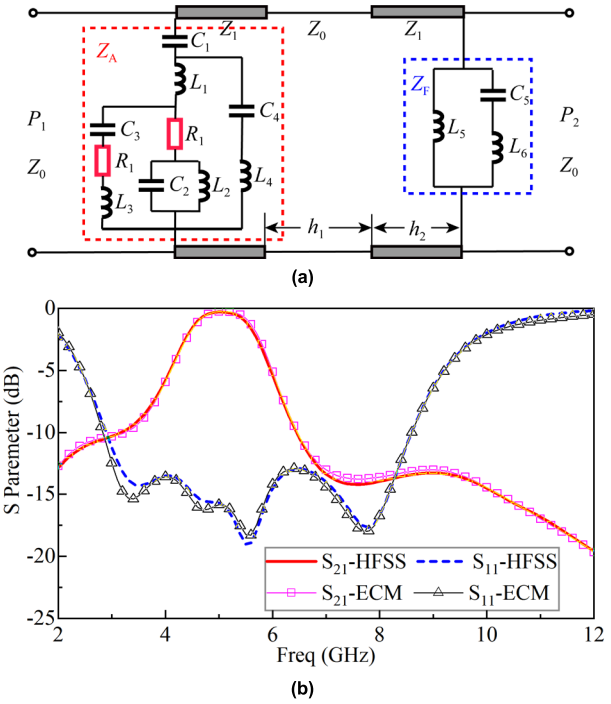


**FIGURE 5.** Equivalent circuits models and Results of ATFSS#1. (a) ECM. (b) S parameter of ATFSS#1.

was divided into four parts and the mutual coupling inevitably exists between the four legs after the lumped resistors were added into the element. In order to make the ECM more accurate in wide band, two additional series circuits ($L_3R_1C_3$ and $L_4C_4$, where $L_4 = L_1' + L_2''$) should be added, as shown in Fig. 4(b).

Fig. 4(c) shows the results of HFSS and ECM. It is evident that the results agree well with each other. The values of the components are $L_1 = 13.32$ nH, $L_2 = 6.41$ nH, $L_3 = 30.31$ nH, $L_4 = 56.07$ nH, $C_1 = 0.0825$ pF, $C_2 = 0.151$ pF, $C_3 = 0.0086$ pF, $C_4 = 0.0014$ pF, $R_1 = 400\ \Omega$, respectively.

Fig. 5(a) shows the ECM of the ATFSS#1. The impedances $Z_0 = 377\ \Omega$ and $Z_1 = Z_0/\sqrt{\varepsilon_r} = 177.8\ \Omega$, respectively. Fig. 5(b) shows the simulation results of ECM and HFSS. A transmission band with a minimum insertion loss of 0.32 dB around 5 GHz is obtained. The figure also shows that the band of $|S_{11}| < -10$ dB covered from 2.9 to 8.5 GHz, which is much wider than the bandwidth of the passband. The results indicate that at the frequency bands around 3.5 GHz and 7.5 GHz, the incident signals which propagate along the $-z$ direction (in Figure 2) are absorbed because both the reflection and transmission coefficients are small.

The following sections presents how we increase the out-of-band rejection at the desired frequency and expand the absorptive bandwidth.

### B. INCREASING THE OUT-OF-BAND REJECTION

Generally speaking, using a multilayer structure can improve the out-of-band rejection during the design of a pass-band FSS; but it is inevitable that the size is enlarged. Another effective way for improving out-of-band rejection at the desired band is to control the location of its transmission zeros. In this design, we added a four-legged loaded slot element into the filter FSS to produce a transmission zero at the high band, on the condition that the length and the width of the square slot did not change. Fig. 6 (a) shows the unit cell structure and its equivalent circuit of the revised version of the bandpass filter FSS. The dimensions are $l_6 = 6$ mm, $l_7 = 1.5$ mm, $g_2 = 0.3$ mm, respectively. The property of the inner cross was initially set as PEC. The four-legged loaded slot element can be modelled with a parallel-series circuit ($L_6C_6$ and $L_7C_7$) [21], which replaces the inductance $L_6$ in Fig. 5(a). The equivalent inductances and capacitances are $L_5 = 2.565$ nH, $L_6 = 0.255$ nH, $L_7 = 1.181$ nH, $C_5 = 0.363$ pF, $C_6 = 0.651$ pF, $C_7 = 0.116$ pF.

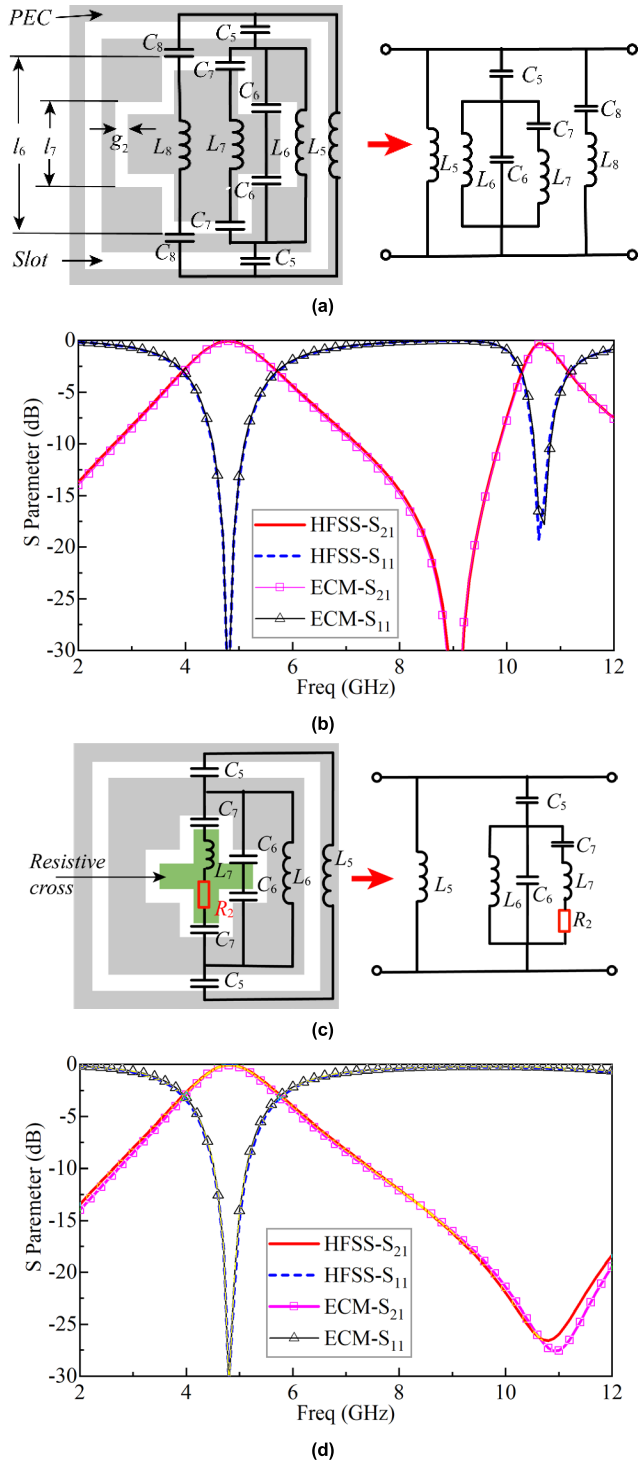


**FIGURE 6.** Equivalent circuits models and Results. (a) Bandpass FSS with PEC. (b) S parameter of the FSS with PEC cross. (c) Bandpass FSS with resistive cross. (d) S parameter of the FSS with resistive cross.

Fig. 5(b) shows the simulation S parameters of HFSS and ECM. It is found that a transmission zero appeared at about 9 GHz; and as a result, the right side of the pass-band was steepened. However, the out-of-band rejection deteriorated with a second transmission band bulge around 10.8 GHz. In order to suppress the second transmission band,

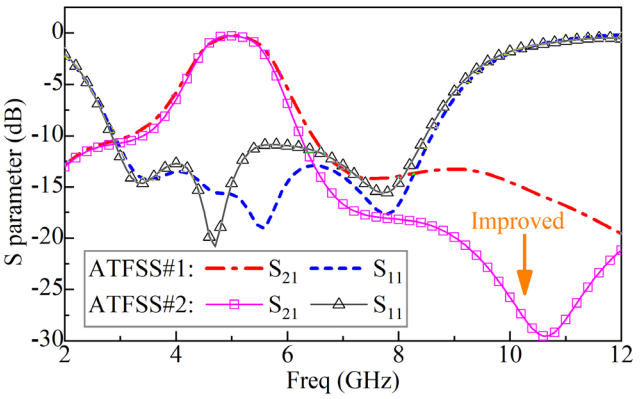


**FIGURE 7.** Simulation results of the ATFSS with improved out-of-band rejection.

a resistive cross with a resistance value of 200 ohm per square, was substituted for the PEC cross in the center. The revised ECM is shown in Fig. 6(c), where the resistor $R_2 = 200\ \Omega$ has been added. The values of the capacitances $C_6$, $C_7$ and inductance $L_7$ are changed due to the material of the inner cross is not perfect conductor. In this case, $C_6 = 0.651$ pF, $C_7 = 0.097$ pF and $L_7 = 1.52$ nH. The simulation results of the filter with the resistive cross are shown in Fig. 6(d). It is evident that the transmission zero shifted from 9 to 11 GHz, and the second transmission band was suppressed or shifted to the higher frequency band. The position of transmission zeros altered with changing the length of the inner cross ($l_6$).

Fig. 7 shows the S parameters of the second ATFSS (ATFSS#2) with the resistive cross. The figure illustrates that the out-of-band rejection was significantly increased within 7-12 GHz after the resistive cross was added. It is worth mentioning that the in-band insertion loss of the FSR with the loaded cross did not change a lot compared with that of the ATFSS#1.

### C. EXPANDING THE ABSORPTIVE BAND

In order to broaden the absorption bands, we redesigned the absorptive FSS to satisfy two basic requirements. First, within the passband, the transmission coefficient, as well as the minimum insertion loss and passband bandwidth, should not be changed significantly. Second, it is better to keep the out-of-band transmission coefficient around $-3$ to $-5$ dB and to keep the reflection efficiency as low as possible.

Our strategy for realizing these requirements was to add one absorptive periodic structure, i.e., loaded dipoles. The new absorptive FSS is shown in Fig. 8(a). Four dipoles, each of which was loaded with a lumped resistor of 200 ohm at the center, were tilted at an angle of 45° in four quadrants of the four-legged loaded element. The position of these dipoles is $l_7 = 6$ mm, $p_1 = 7$ mm. The simulated transmission and reflection performance of the FSS with four loaded dipoles is shown in Fig. 8(b). Varying the length of the dipole, together with the resistance of the lumped resistor, did not significantly change the insertion loss below 8 GHz, and the insertion loss

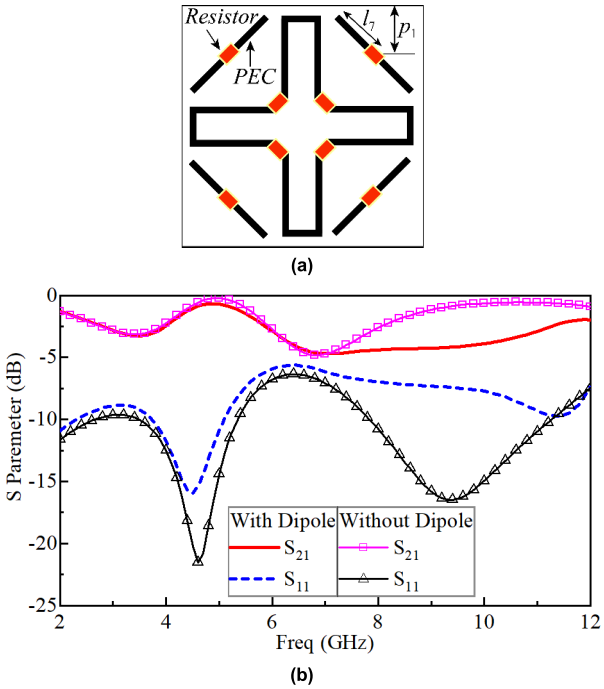


**FIGURE 8.** Wideband absorptive FSS. (a) Structure. (b) S parameters.

increased to about 3 - 5 dB and remained stable in 8-12 GHz. Although the change of $S_{11}$ was noticeable, it was still less than $-5$ dB in whole bands.

### D. RESULTS OF ATFSS WITH WIDE ABSORPTIVE BAND

To evaluate the performance of the third ATFSS (ATFSS#3), Fig. 9 (a) and (b) show the structure and the simulation results, respectively. As shown in Fig. 9 (b), the upper absorptive bandwidth was expanded greatly. The band of $|S_{11}| < -10$ dB covered from 3 to 11.5 GHz, which is much wider than that of ATFSS#2. Due to the absorption of the loaded dipoles, the minimum in-band insertion loss increased from 0.32 to 0.6 dB, but the out-of-band rejection improved in 8-10.5 GHz. It is worth to mention that the total thickness of the ATFSS was reduced because the space $h_1$ was cut from 8.4 mm to 6.4 mm.

The cross resistive cross can be replaced with lumped resistors. In this design, each cross is split at the intersection point and connected with four lumped resistors of 200 ohm; and the material of the cross is set as a perfect conductor, as shown in Fig. 10 (a). The simulation results of the fourth ATFSS (ATFSS#4) are shown in Fig. 10 (b). After the cross was replaced by the lumped resistors, the bandwidth of the passband and the absorption band remained nearly unchanged, only the out-of-band rejection at high frequencies showed small changes.

## III. DISCUSSIONS OF EXPERIMENTAL RESULTS

To verify the designs and simulation results discussed above, a prototype of the proposed ATFSS#4 was fabricated. Both FSSs were etched on substrates (Arlon AD450) with a thickness of 0.794 mm, permittivity of 4.5, and loss

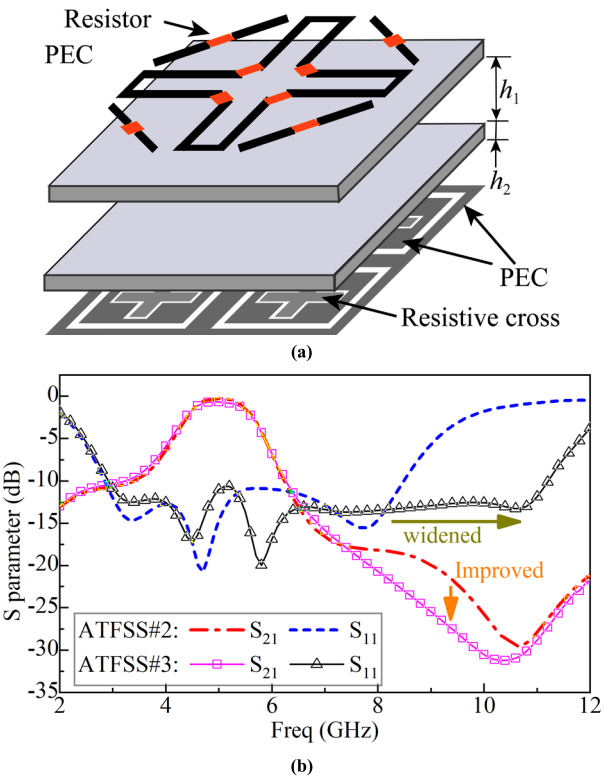


**FIGURE 9.** ATFSS with loaded dipoles. (a) Structure. (b) S parameters.

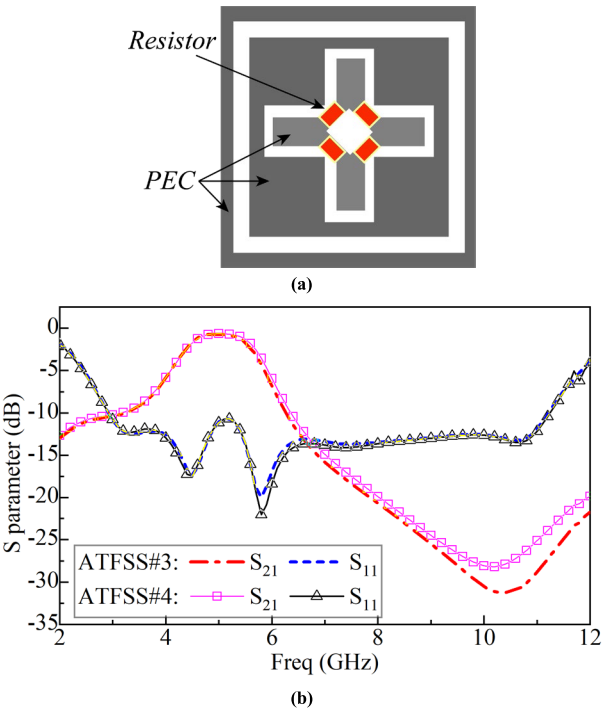


**FIGURE 10.** ATFSS with center cross loaded by lumped resistors. (a) Structure. (b) S parameters.

tangent 0.0035. The overall size of the fabricated structure was 200 mm $\times$ 200 mm, on which 256 units of loaded dipoles, 64 units of four-legged loaded elements, 256 units

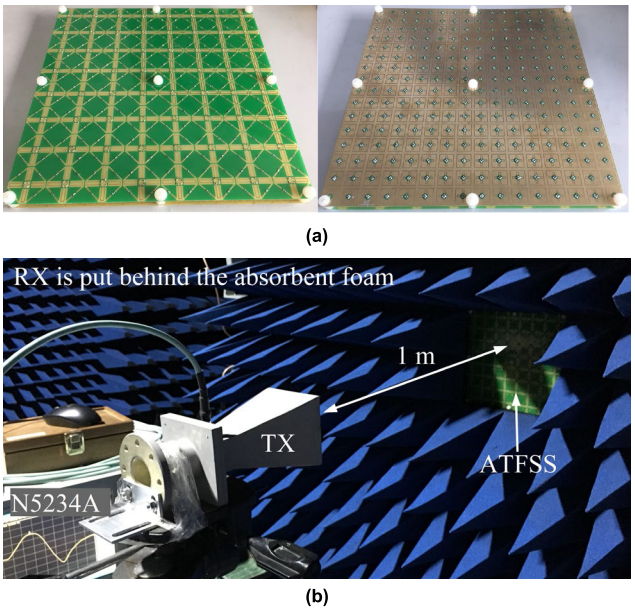


**FIGURE 11.** Prototype and experimental system. (a) Photo of the prototype. (b) Measurement setup.

of loaded crosses were printed and 1,536 chip resistors were soldered. Plastic pillars and screws were used to fix the essential 6.4 mm air gap between the two layers. A photo of the ATFSS#4 is shown in Fig. 11(a).

Fig. 11(b) shows the measurement setup. The ATFSS was measured in an anechoic chamber by using Keysight N5234A with the time-domain gating. The aperture of two horn antennas for testing is 75 mm × 75 mm. The space between transmitting antenna (TX) or receiving antenna (RX) and the ATFSS was 1 m. The ATFSS was surrounded with the absorbent foam to reduce the effect of the edge diffraction. Due to the measurement set-up limitation, the far-field condition was hard to meet for the entire frequency range. Our prototype was positioned on the far field of the TX antennas so that the transmission can be considered similar to the simulation. Time-domain gating was used during measuring the reflection coefficient to reduce the multipath interferences.

A comparison of the simulated and measured transmission and reflection coefficients under the normal incidence is shown in Fig. 12(a). A relatively good agreement in the passband but some discrepancy in the absorption band is exhibited. The measured transmission zero is lower than that of simulation. The possible reason is that the package and solder of the resistors have not been taken into account in the simulation. The main factor of the large difference at the low frequency, below 3 GHz, is because the overall size of the FSS was not larger than 2λ. The measurement bandwidth of the passband with $|S_{21}| \geq -3$ dB was from 4.25 to 5.65 GHz, with a minimum insertion loss of 0.92 dB. The reflection coefficients were below - 10 dB in the range of 2.8 to 11.4 GHz, which was 4 octave bandwidth.

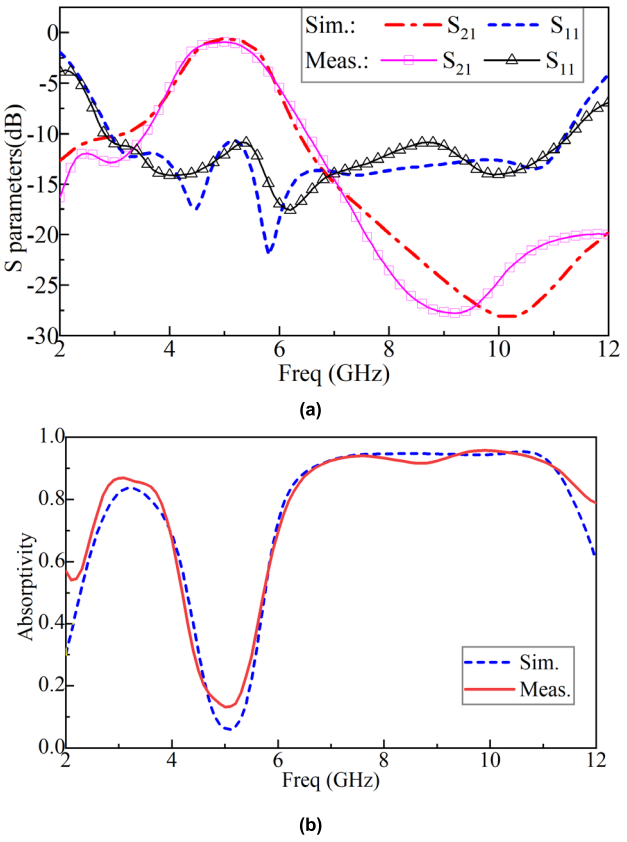


**FIGURE 12.** Measurement and simulation results. (a) S parameters. (b) Absorptivity.

**TABLE 1.** Performance comparison.

| Ref. | Bands of A>80% (GHz) | | $f_c$[1] (GHz) | $IL_{min}$[2] (dB) | Thickness @$\lambda_{AL}$[3] |
|---|---|---|---|---|---|
| | Low band | High band | | | |
| [9] | 3.76-8.7 | 12-16.08 | 10.3 | 0.3 | 0.112 |
| [10] | 2.5-3.2 | 6.05-6.79 | 4.42 | 0.68 | 0.108 |
| [11] | 3.61-6.12 | 6.98-10.17 | 6.74 | 2.45 | 0.108 |
| [13] | 1.79-2.6 | 4.5-5.25 | 3.68 | 1.28 | 0.127 |
| [15] | 2.66-4.5 | 5.66-8.56 | 5 | 0.35 | 0.098 |
| [16] | N.A. | N.A. | 4.52 | 0.73 | 0.098 |
| This work | 2.7-3.8 | 6.2-11.7 | 5 | 0.92 | 0.072 |

[1] $f_c$: Center frequency of passband.
[2] $IL_{min}$: The minimum insertion loss of passband.
[3] $\lambda_{AL}$: Wavelength of the lowest frequency of absorption band.

Using the equation, $A = 1 - |S_{11}|^2 - |S_{21}|^2$, the absorptivity $A$ is calculated. Fig. 12(b) shows the comparison of simulation and measurement of the absorptivity under the normal incidence. It is noted that the two absorption bands located at two sides of the passband are seen. The lower and higher absorption bandwidths with an absorption rate higher than 80% were 33.8% (2.7 to 3.8 GHz) and 61.5% (6.2 to 11.7 GHz), respectively.

The comparisons between the proposed ATFSS and other published ATFSSs are shown in Table 1. All ATFSSs listed in the table have a band of $|S_{11}| < -10$ dB which includes

a passband and absorptive bands. Apparently, compared with all other works listed in the table, the fractional bandwidth of this work is the maximum and the thickness corresponding to the lowest absorptive frequency is the minimum.

## IV. CONCLUSION

We have presented four ATFSSs with a transparent band in between two wide absorption bands. By cascading a four-legged loaded element FSS and square slot FSS, an ATFSS with two absorption bands that were below and above a passband was obtained. A four-legged loaded slot element, together with a resistance loaded cross was added into a square slot FSS to increase the out-of-band rejection at the high absorption band. In order to expand the absorption band, loaded dipoles were added. After the ATFSS was elaborately designed, one prototype was fabricated using printed circuit board technology to verify the design. The measured results showed that a passband of 3 dB bandwidth covering from 4.25 to 5.65 GHz and a low reflection band of $|S_{11}| < -10$ dB ranging from 2.8 to 11.4 GHz were obtained. Within the low reflection band, two wide absorption bands with an absorption rate higher than 80% were achieved.

## REFERENCES

[1] B. A. Munk, *Metamaterials: Critique and Alternatives*. Hoboken, NJ, USA: Wiley, 2009.
[2] W. S. Arceneaux, R. D. Akins, and W. B. May, "Absorptive/transmissive radome," U.S. Patent 5 400 043, May 21, 1995.
[3] Z. Shen, J. Wang, and B. Li, "3-D frequency selective rasorber: Concept, analysis, and design," *IEEE Trans. Microw. Theory Techn.*, vol. 64, no. 10, pp. 3087–3096, Oct. 2016.
[4] A. Motevasselian and B. L. G. Jonsson, "Design of a wideband rasorber with a polarisation-sensitive transparent window," *IET Microw., Antennas Propag.*, vol. 6, no. 7, pp. 747–755, May 2012.
[5] F. Costa and A. Monorchio, "A frequency selective radome with wideband absorbing properties," *IEEE Trans. Antennas Propag.*, vol. 60, no. 6, pp. 2740–2747, Jun. 2012.
[6] B. Yi, L. Yang, and P. Liu, "Design of miniaturized and ultrathin absorptive/transmissive radome based on interdigital square loops," *Prog. Electromagn. Res. Lett.*, vol. 62, pp. 117–123, Sep. 2012.
[7] Q. Chen, L. Liu, L. Chen, J. Bai, and Y. Fu, "Absorptive frequency selective surface using parallel LC resonance," *Electron. Lett.*, vol. 52, no. 6, pp. 418–419, Mar. 2016.
[8] Q. Chen, S. Yang, J. Bai, and Y. Fu, "Design of absorptive/transmissive frequency-selective surface based on parallel resonance," *IEEE Trans. Antennas Propag.*, vol. 65, no. 9, pp. 4897–4902, Sep. 2017.
[9] Q. Chen, D. Sang, M. Guo, and Y. Fu, "Frequency-selective rasorber with interabsorption band transparent window and interdigital resonator," *IEEE Trans. Antennas Propag.*, vol. 66, no. 8, pp. 4105–4114, May 2018.
[10] Y. Shang, Z. Shen, and S. Xiao, "Frequency-selective rasorber based on square-loop and cross-dipole arrays," *IEEE Trans. Antennas Propag.*, vol. 62, no. 11, pp. 5581–5589, Nov. 2014.
[11] K. Zhang, W. Jiang, and S. Gong, "Design bandpass frequency selective surface absorber using LC resonators," *IEEE Antennas Wireless Propag. Lett.*, vol. 16, pp. 2586–2589, Nov. 2017.
[12] H. Huang and Z. Shen, "Absorptive frequency-selective transmission structure with square-loop hybrid resonator," *IEEE Antennas Wireless Propag. Lett.*, vol. 16, pp. 3212–3215, Nov. 2017.
[13] Y. Han, W. Che, X. Xiu, W. Yang, and C. Christopoulos, "Switchable low-profile broadband frequency-selective rasorber/absorber based on slot arrays," *IEEE Trans. Antennas Propag.*, vol. 65, no. 12, pp. 6998–7008, Oct. 2017.
[14] M. Guo, Z. Sun, D. Sang, X. Jia, and Y. Fu, "Design of frequency-selective rasorbers based on centrosymmetric bended-strip resonator," *IEEE Access*, vol. 7, pp. 24964–24970, 2019. doi: 10.1109/ACCESS.2019.2893347.
[15] Q. Guo, Z. Li, J. Su, Y. L. Yang, and J. Song, "Dual-polarization absorptive/transmissive frequency selective surface based on tripole elements," *IEEE Antennas Wireless Propag. Lett.*, vol. 18, no. 5, pp. 961–965, May 2019. doi: 10.1109/LAWP.2019.2906675.
[16] X. Xiu, W. Che, Y. Han, and W. Yang, "Low-profile dual-polarization frequency-selective rasorbers based on simple-structure lossy cross-frame elements," *IEEE Antennas Wireless Propag. Lett.*, vol. 17, no. 6, pp. 1002–1005, Jun. 2018.
[17] Q. Chen, D. Sang, M. Guo, and Y. Fu, "Miniaturized frequency-selective rasorber with a wide transmission band using circular spiral resonator," *IEEE Trans. Antennas Propag.*, vol. 67, no. 2, pp. 1045–1052, Feb. 2019.
[18] M. Qu, S. Sun, L. Deng, and S. Li, "Design of a frequency-selective rasorber based on notch structure," *IEEE Access*, vol. 7, pp. 3704–3711, 2019. doi: 10.1109/ACCESS.2018.2886421.
[19] Y. Ma, W. Wu, Y. Yuan, W. Yuan, and N. Yuan, "A high-selective frequency selective surface with hybrid unit cells," *IEEE Access*, vol. 6, pp. 75259–75267, 2018. doi: 10.1109/ACCESS.2018.2878941.
[20] F. Costa, A. Monorchio, and G. Manara, "Efficient analysis of frequency selective surfaces by a simple equivalent-circuit model," *IEEE Antennas Propag. Mag.*, vol. 54, no. 4, pp. 35–48, Aug. 2012.
[21] Q. Guo, Z. Li, J. Su, J. Song, and L. Y. Yang, "Active frequency selective surface with wide reconfigurable passband," *IEEE Access*, vol. 7, pp. 38348–38355, 2019. doi: 10.1109/ACCESS.2019.2906219.

**QINGXIN GUO** (SM'12) received the B.S., M.S., and Ph.D. degrees in electromagnetic field and microwave technology from Communication University of China, Beijing, China, in 1997, 2006, and 2013, respectively. From 1997 to 2002, he was an Engineer of Xiamen Overseas Chinese Electronics Company, Ltd., where he was involved with the repeaters and the mobile phone for the GSM system. From 2002 to 2004, he was a Project Manager of Beijing Gigamega Electronics Company, Ltd., where he was responsible for the design of amplifier for transmitter. From 2004 to 2008, he was an Engineer and a Project Manager of Beijing Filcom Technology Company Ltd., where he was responsible for the design of combiner and multiplexer. In 2006, he joined Communication University of China, where he has been an Associate Professor with School of Information Engineering, since 2013. From 2011 to 2012, he was a Visiting Researcher of Electromagnetic Communication Laboratory (EMC lab) which is affiliated with Electrical Engineering Department, Pennsylvania State University. His research interests include the antennas, microwave passive components, RF circuits and metamaterial.

**JIANXUN SU** received the B.S. degree in electronic information engineering from Taiyuan University of Technology, Taiyuan, China, in 2006, the M.S. and the Ph.D. degrees in electromagnetic field and microwave technology from the Communication University of China and Beijing Institute of Technology, Beijing, China, in 2008 and 2011, respectively. From 2012 to 2014, he was with China Electronics Technology Group Corporation (CETC), where he engaged in phased-array system research. He is currently working as an Associate Researcher with the School of Information Engineering, Communication University of China and also with the Science and Technology on Electromagnetic Scattering Laboratory. His special research interests include integral equation method, metamaterial, phased-array antenna, and radar target characteristics.

**ZENGRUI LI** received the B.S. degree in communication and information system from Beijing Jiaotong University, Beijing, China, in 1984, the M.S. degree in electrical engineering from Beijing Broadcasting Institute, Beijing, China, in 1987; and the Ph.D. degree in electrical engineering from Beijing Jiaotong University, Beijing, China, in 2009. He has studied in Yokohama National University, Japan, from 2004 to 2005. He is currently a Professor with the Communication University of China, Beijing, China. He is a Senior Member of Chinese Institute of Electronics. His research interests include the areas of computational electromagnetics, the finite-difference time-domain methods, electromagnetic modeling and simulation of antennas, and communication antennas.

**LAMAR Y. YANG** (S'02–M'09–SM'09) received the B.S. degree from the Northern Jiaotong University, China, and the M.S. degree from the Beijing Broadcast Institute, China, all in electrical engineering. He received the Ph.D. degree in the area of wireless communications and networks from the University of Texas (UT) at Austin, in 2006. He is currently an Associate Professor with the Department of Computer and Electronics Engineering, University of Nebraska-Lincoln (UNL). Dr. Yang has served as a Technical Program Committee (TPC) member for many years for numerous top ranked conferences, such as Globecom, ICC, VTC, WCNC, MSWiM, etc., and he served as a Reviewer for the IEEE TRANSACTIONS ON WIRELESS COMMUNICATIONS (TWC), Vehicular Technology (TVT), Circuits and Systems for Video Technology (TCSVT), Communications Letters, etc. His current research interests include wireless communications and networks with emphasis on radio channel characterizations, cognitive radio networks, and statistical signal processing.

**JIMING SONG** (S'92–M'95–SM'99–F'14) received the B.S. and M.S. degrees in physics from Nanjing University, Nanjing, China, in 1983 and 1988, respectively, and the Ph.D. degree in electrical engineering from Michigan State University, East Lansing, MI, USA, in 1993. From 1993 to 2000, he was a Postdoctoral Research Associate, a Research Scientist, and a Visiting Assistant Professor with the University of Illinois at Urbana-Champaign, Champaign, IL, USA. From 1996 to 2000, he was a Part-Time Research Scientist with SAIC-Champaign, (formerly Demaco, Inc.), Champaign. He was a Principal Staff Engineer/Scientist with Semiconductor Products Sector of Motorola, Tempe, AZ, USA. In 2002, he joined the Department of Electrical and Computer Engineering, Iowa State University, Ames, IA, USA, as an Assistant Professor, where he is currently a Professor. He has authored the Fast Illinois Solver Code. His current research interests include the modeling and simulations of interconnects on lossy silicon and RF components, electromagnetic wave scattering using fast algorithms, the wave propagation in metamaterials, acoustic and elastic wave propagation and nondestructive evaluation, and transient electromagnetic field. Dr. Song is an ACES Fellow. He was selected as a National Research Council/Air Force Summer Faculty Fellow in 2004 and 2005. He was a recipient of the NSF Career Award in 2006. He is an Associate Editor of the IEEE ANTENNAS AND WIRELESS PROPAGATION LETTERS and ACES Express.